ELASTIC MODULI, AND ESTIMATIONS OF SOME PHYSICAL, THERMAL, AND OPTICAL PARAMETERS OF GE-SE-AS GLASSY SYSTEMS WITH IMPROVED MECHANICAL STRENGTH

Reference NO. IJME 1354, DOI: 10.5750/ijme.v1i1.1354

Dipankar Biswas*, Department of Electronics and Communication Engineering, Institute of Engineering and Technology, GLA University, Mathura, UP 281406, India, **Rittwick Mondal,** Department of Physics, Chowhatta High School, Birbhum 731201, India, **Souvik Brahma Hota**, Department of Mechanical Engineering, Techno India University, Kolkata 700091, West Bengal, India, **Rahul Singh,** Chitkara Centre for Research and Development, Chitkara University, Himachal Pradesh, India and **Rishu Chabra,** Centre of Research Impact and Outreach, Chitkara University, Rajpura, Punjab, India

* Corresponding author. Dipankar Biswas (Email): biswas.dipankar3579@gmail.com

KEY DATES: Submission date: 08.12.2023 / Final acceptance date: 21.02.2024 / Published date: 12.07.2024

SUMMARY

Employing the melt quench approach, glassy systems with the chemical composition $Ge_{30}Se_{(70-x)}As_x$ have been synthesized. As the amount of arsenic increases, various physical, mechanical, thermal, optical parameters and some other aspects of elastic moduli have been assessed. The XRD pattern shows the amorphous characteristics of the inspected materials. The density of the glasses increases from 4.32 to 4.61 g-cm^{-3} whereas the molar volume declines from 19.32 to 18.62 cm^3 mol^{-1} as the concentration of arsenic increases. The measured values of the ultrasonic velocities have been used to measure the elastic properties, such as the Shear, and longitudinal strains, Bulk modulus, Young's modulus, and Poisson's ratio of the synthesized glasses. The upsurge in the values of elastic moduli indicated the upgrading in the elastic properties of the materials. The outcomes are interpreted in terms of a profound structural change brought about by molecular rearrangement, which regulates the glass's physical characteristics. The optical band gap energies are found to decrease from 2.17 to 1.86 eV due to the increase in Urbach energies from 040 to 0.64 eV with the incorporation of arsenic atom. The obtained results indicate the perspective of the as-synthesized thermally stable materials to be used in optoelectronic devices.

KEYWORDS

Chalcogenide glass, Elastic moduli, Glass transition temperature, Optical band gap energy

1. INTRODUCTION

The outstanding physical, optical, and technological uses of chalcogenide multicomponent glasses have garnered significant attention (Mohamed et al., 2023, Chauhan et al., 2023, Lee et al., 2021). They are regarded as standard infrared glasses and make excellent choices for sensors, thermoelectric devices, non-linear photonics, and sophisticated infrared optical fibres (Kang et al., 2022, Wang et al., 2023, Choyon and Chowdhury, 2022, Kibler et al., 2023). They also offer fresh approaches to the difficult basic issues pertaining to the potential technical uses of these glasses for solid-state physicists (Pitchappa et al., 2019). Because of its strong glass-forming capabilities, pure selenium has long been a favored host matrix among chalcogenides (Kumar et al., 2019). Nevertheless, pure Se has certain drawbacks, such as limited sensitivity and a brief lifespan. Researchers alloy Se with a few favored additions, such as Cd, Zn, In, Ge, Cu, Sb, Bi, etc., to overcome this constraint (Hassanien and Sharma, 2024). Tetrahedral-coordinated geometry is acquired by the additional structural units present in the chalcogenide glasses containing Ge as one of its constituents (Pal et al., 2019). The glass-forming tendency is enhanced when Ge joins a parent element (Hassanien et al., 2020b). Furthermore, the emergence of cross-linked structural units of Ge with long polymeric chains of Se reduces physical ageing. By raising the mean bond energy, these characteristics strengthen the mean of the glass network (Boukhris et al., 2020). Consequently, the main factor in bond modification is Ge inclusion. Ge's electro-negativity values and size complement each other perfectly, resulting in a very stable glass-forming liquid (Mondal et al., 2023). Given these characteristics, Ge is selected as the network's host matrix since it improves the glass-forming region and has strong stability against crystallization (Vashist et al., 2022). While it reduces the impacts of ageing, alloying Se and Ge with As improves the glass-forming region and thermal stability. Of all the components that make up the chalcogenide family, the glass that has the As-Se combination is the most important since it has a wide variety of optical qualities and is used in numerous applications (Yang et al., 2010). The physical, structural, thermal, and optical characteristics of Se-Ge-Te (Chahal

and Ramesh, 2022), Se-As-Te (Delaizir et al., 2011), and As-Se-Bi (Biswas et al., 2023) chalcogenide glasses have been documented by a number of researchers in earlier investigations. On the other hand, it appears that not many studies on physio-chemical, spectroscopic, and mechanical analyses of Ge-Se glassy matrix doped with As atom have been published. Ge-Se-As ternary was chosen by the writers for the current study for this reason.

Examining the impact of Arsenic incorporation on various physical, thermal, and optical parameters as a result of arsenic doping into the Ge-Se host matrix is the main goal of this report. This study's key objective is to examine different mechanical parameters such as the prepared glasses' elastic moduli Bulk (K), Young (Y), and Poisson's ratio (P_r). These parameters are found using the density (ρ) and the ultrasonic velocities (longitudinal and transverse, v_L and v_T). In addition, this work seeks to determine the impact of arsenic incorporation on the examined glassy systems' physio-chemical parameters. Moreover, this study examines the possible applicability of the as-synthesized material for optical device design.

2. EXPERIMENTAL DETAILS AND METHODOLOGY

2.1 SAMPLES PREPARATION

Arsenic-incorporated $Ge_{30}Se_{(70-x)}As_x$ (2,4,6, and 8 at%) stoichiometrically mixed bulk samples have been created by utilizing the well-known melt quenching process, which is elucidated in detail elsewhere (Hammad and Abdelghany, 2016).

2.2 CHARACTERIZATION TECHNIQUE

For the structural study of the materials as prepared, a sophisticated X-ray diffractometer (Model: Rigaku TTRAX-III) equipped with a Cu target with a wavelength of 1.5419 Å was used. The X-ray diffraction measurements were carried out at a speed of one half-minute and within a scan range of 10º–80º.

2.3 DENSITY AND MOLAR VOLUME MEASUREMENT

The non-reactive immersing liquid used was acetone, and the densities of each glass were determined using the well-known Archimedes method (Saddeek et al., 2010).

$$\rho = \rho_{acetone}\left(\frac{W_{air}}{W_{air} - W_{acetone}}\right) \quad (1)$$

In this instance, W_{air} and $W_{acetone}$ represent acetone and the weight of glasses suspended in midair, respectively. The symbol $\rho_{acetone}$ represents the density of acetone. With the molecular weight (M) and ρ (Eq. (1)) values known, the formula (Eq. (2)) has been shaped to calculate the molar volume (V_M) of the glass samples (Saddeek et al., 2010).

$$V_M = \sum \frac{x_i M_i}{\rho} \quad (2)$$

In this instance, x_i and M_i stand for the molecular weight and molar fraction of the i^{th} glass composite, respectively.

2.4 MEASUREMENTS OF ELASTIC MODULI

An ultrasonic flow detector (USN 60) using the pulse-echo-overlap technique has been used to achieve the ultrasonic measurements in our study at room temperature. The ultrasonic velocity (v) can be obtained by following the steps by reading and selecting the first two echo signals with amplitudes A_1, A_2, and the corresponding times t_1, t_2 generated in the sample (Saddeek et al., 2020),

$$\upsilon = \frac{2X}{t_2 - t_1} \quad (3)$$

In this instance, t is the pulse time (s) and X is the sample thickness. The shear (S) and longitudinal (L) strains were calculated using the measured $\boldsymbol{v}_L$, $\boldsymbol{v}_T$ and ρ values in accordance with the following rel*a*tions: $L = \rho \boldsymbol{v}_L^2$, and $S = \rho \boldsymbol{v}_L^2$.The Poisson ratio ($P_r$), Young (Y), and Bulk (K) moduli were calculated by calculating the S and L values in the manner described below (Saddeek et al., 2020, Mondal et al., 2021a):

$$K = L - 1.33S \quad (4)$$

$$P_r = (L - 2S)(2L - 2S)^{-1} \quad (5)$$

$$Y = 2S(1 + P_r) \quad (6)$$

2.5 THERMAL MEASUREMENTS

For the DSC thermogram measurements, a Shimadzu-50 calorimeter were used, with a continuous heating rate of 10K/min, in the temperature range of 300 to 700 K.

2.6 OPTICAL MEASUREMENTS

The UV-visible spectra of the polished glass samples were measured at room temperature using a Shimadzu UV-1800 series spectrophotometer, covering wavelengths ranging from 200 to 800 nm. To calculate the absorption coefficient α(v) at the spectrum edge area, by using Eq. (7) (Singh et al., 2021b, Davis and Mott, 1970):

$$\alpha(\nu) = (2.303/d)A(\nu) \quad (7)$$

In this discussion, 'd' represents the sample thickness, and 'A' indicates the amount of light absorbed. A power law that helps illustrate how amorphous materials absorb light, particularly above the exponential tail, is explained by Eq. (8). According to Davis and Mott , this instance has a larger value of α(υ) (Hafiz et al., 2007).

$$\alpha h\nu = A(h\nu - E_g)^n \quad (8)$$

It is possible to assume that different values for the index 'n', such as 2, 3, 1/2, and 1/3, correspond to different sorts of transitions, such as direct allowed/forbidden and indirect allowed/forbidden. In this case, 'A' stands for the band tailing parameter, 'E_g' for the optical band gap energy, and 'hν' for the incident photon energy.

3. RESULT AND DISCUSSION

3.1 X-RAY DIFFRACTION

As illustrated in Figure 1, the XRD patterns of the $Ge_{30}Se_{(70-x)}As_x$ samples depicts no significant peaks apart from the broad peak owing to glass structure.

The obtained pattern of the studied materials shows merely a broad hump between 20 and 40 degrees, with no acute peak connected to crystallinity. This observation could be explained by the studied samples' non-crystalline, amorphous nature or short-range order (Hassanien et al., 2020a).

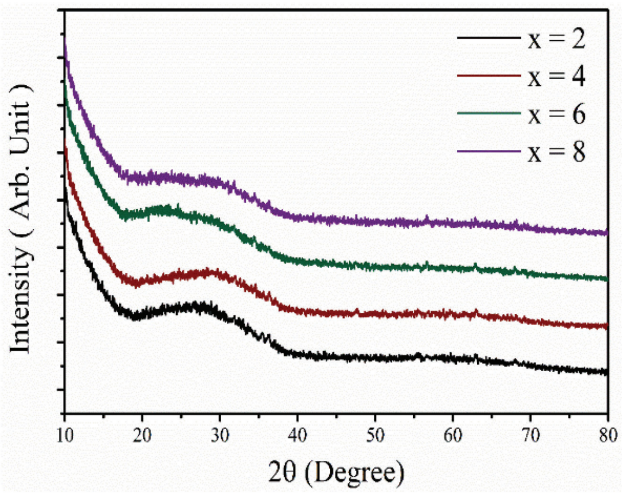

Figure1. XRD patterns of $Ge_{30}Se_{(70-x)}As_x$ glassy systems

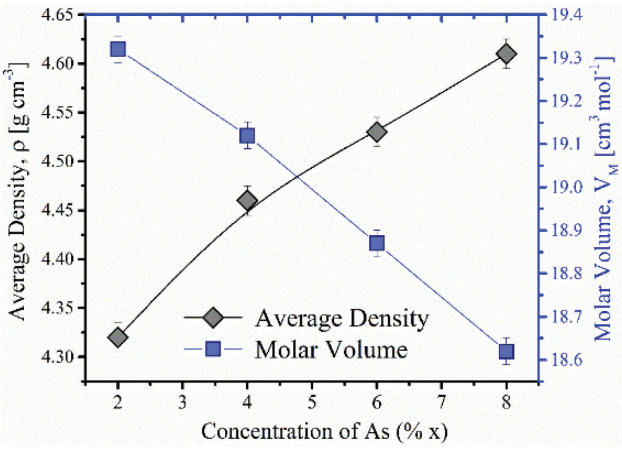

Figure 2. Variation of density and molar volume with Arsenic content(x)

3.2 STUDY OF DENSITY AND MOLAR VOLUME

When examining the structural alterations of the geometrical configurations in the glass network, density is a crucial quantity to consider. It also clarifies the glass network's level of structural compactness. In addition, density aids in the assessment of numerous significant thermal, elastic, and optical characteristics. Eq. (1) is used to measure the sample densities.

The computed density (ρ) values are plotted versus the Arsenic concentration (x) in Figure 2. The molar volume, another crucial measure for analyzing the structural characteristics of the materials, is correlated with density. Eq. (2) can be used to find the glassy system's molar volume. As shown in some earlier research, it is evident from Figure 2 that there is an inverse relationship between density and molar volume. According to a prior report, the higher-density As (5.72 g/cm³) atoms may have replaced the lower-density Ge (5.32 g/cm³) and Se (4.81 g/cm³) elements, which is why ρ increased (Yadav et al., 2019). Conversely, the inclusion of the Arsenic atom, which has a lower atomic radius (R_{As} = 1.16 Å, rather than Ge and Se, which have greater atomic radii (R_{Se} = 1.22 Å and R_{Ge} = 1.52 Å), is responsible for the decrease in V_m.

3.3 STUDY OF ULTRASONIC WAVE VELOCITIES AND ELASTIC MODULI

Table 1 lists the longitudinal velocity (v_L) and shear velocity (v_T) data that were acquired and recorded at room temperature. Figure 3 shows how the As content varies with longitudinal and shear velocities.

Interestingly, when more Arsenic atoms are introduced to the glassy matrix, both v_L and v_T increase from 2657 m/s to 2752 m/s and from 1564 m/s to 1625 m/s, respectively. It has been proposed that structural changes and modifications to the cross-link densities of the glasses under study are the cause of this rise in ultrasonic velocities, which results in a decrease in the propagation of waves through the glass. As shown in Table 2, the computed longitudinal modulus (L) and shear modulus (S) increase from 11.30 to 11.40 Gpa, and the values of the bulk modulus (K), Young's modulus (Y), and Poisson ratio (Pr) likewise show an increasing trend with the addition of the Arsenic atom. An essential mechanical measure for examining how a substance compresses under external pressure is the elasticity bulk modulus. The elastic moduli are extremely significant parameter for a material to inspect to examine the functionalization of that sample (Bhutto et al., 2023, Yang et al., 2010). It has previously been noted that with the increase concentration, the elastic moduli also increases for the As-Se system (Ota et al., 1978). The

defect homopolar Se-Se bonds in these glasses diminish as arsenic concentrations rise, which affects the elastic moduli's values. It has been demonstrated in the literature that even trace amounts of arsenic can change average connectivity, which in turn can change crosslink density and, in turn, elastic moduli (Mondal et al., 2021b). The Table 1 illustrates how increasing the Arsenic content (x) results in an increase in the mechanical parameters, indicating a rise in glass stiffness. These findings could be explained by the topological analyses of the glasses under study as well as the distribution of chemical bonds.

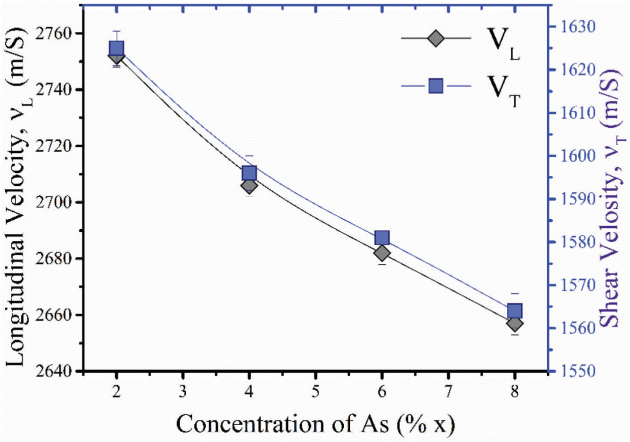

Figure 3. Variation of longitudinal velocity ($\mathbf{v}_L$), and shear velocity ($\mathbf{v}_T$) of studied glasses with Arsenic content(x)

Table 1. The mechanical parameters of the studied glass having composition $Ge_{30}Se_{(70-x)}As_x$ (2,4,6, and 8)

X	v_L m/s	v_T m/s	S Gpa	L Gpa	K Gpa	P_r Gpa	Y Gpa
2	2657	1564	11.30	32.54	17.51	0.196	27.00
4	2682	1581	11.32	32.58	17.52	0.196	27.07
6	2706	1596	11.36	32.65	17.54	0.197	27.19
8	2752	1625	11.40	32.71	17.56	0.198	27.31

3.4 THERMAL STUDY

Figure 4 displays the complete DSC curves for the $Ge_{30}Se_{(70-x)}As_x$ (2,4,6, and 8) glasses recorded at 10 K/min. The homogeneity of the prepared bulk glasses is confirmed by the appearance of one T_g in the DSC curve for each composition. The amorphous-crystalline transitions are represented by the observed exothermic peak. Table 3 tabulates the measured values of the different thermal parameters. The glass transition temperature is observed to drop as the concentration of Arsenic(x) increases (Figure 4).

These curves can be distinguished by their glass transition temperature (T_g), crystallization temperature (T_c), and peak crystallization temperature (T_p). The graph exhibits an endothermic step at the glass transition temperature, with an exothermic second peak resulting from phase change (Shukla and Sharma, 2019). This temperature, which occurs when amorphous material begins to crystallize, is referred to as the crystallization temperature. It has been noted that T_g, T_c, and T_p values drop as Arsenic concentration rises. The correlation between the Arsenic concentration and the changes in the derived density (ρ) values and the thermal stability parameter ($\Delta T=T_c-T_g$) is depicted in Figure 5 (Nian et al., 2018).

Table 2. Measured thermal parameters of the studied glasses with composition $Ge_{30}Se_{(70-x)}As_x$ (2,4,6, and 8)

x	T_g (K)	T_C (K)	T_P (K)	Thermal Stability ($\Delta T=T_c-T_g$) (K)
2	554	691	710	137
4	546	686	705	140
6	533	675	690	142
8	526	663	678	152

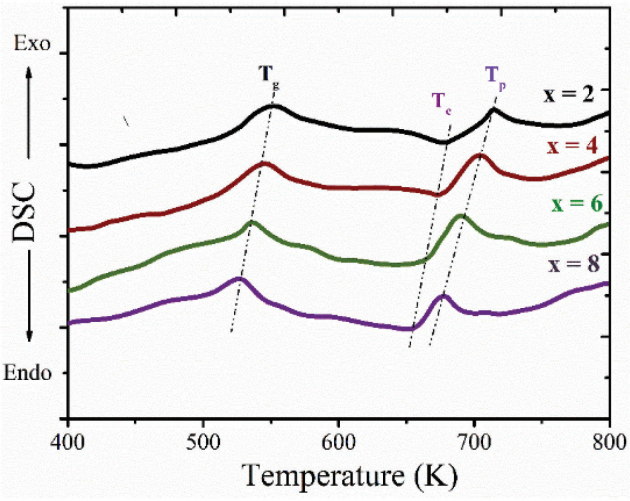

Figure 4. Variation of T_g, T_c, T_p of studied glasses

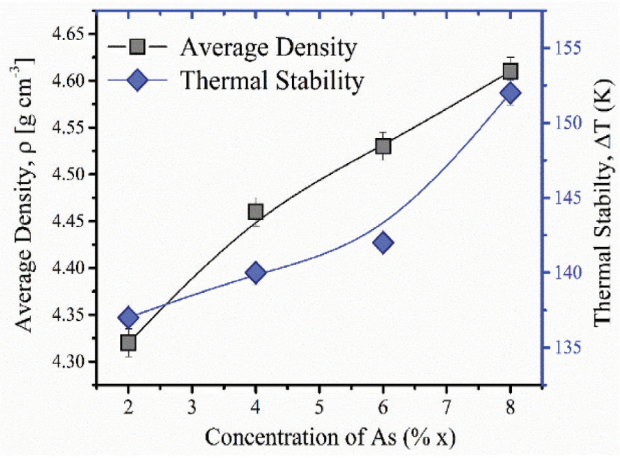

Figure 5. Variation of density, and thermal stability with Arsenic content(x)

It should be noted that the samples exhibit thermal stability across a significant temperature range, suggesting that high-temperature applications could benefit from their use. The glasses' inverse relationship between T_g and ρ makes it evident that adding Arsenic content reduces T_g while increasing ρ. T_g and T_c values drop as the concentration of Arsenic atom increases. Filling the interstitial gaps with arsenic atoms lowers the number of vacancies in the glass matrix and raises the effective density (ρ) value (Biswas et al., 2020). An increase in the Arsenic content of the examined glass demonstrated greater stability against crystallization, as shown by an increase in (T_c-T_g).

3.5 STUDY OF OPTICAL BAND GAP ENERGY AND URBACH ENERGY

The absorption edge in disordered materials tends to be attributed to indirect transitions across an optical gap at elevated absorption coefficient values, according to the electronic structure theory of amorphous materials. Davis and Mott noted that the majority of amorphous semiconductors permit direct transitions, with a corresponding value of 'n' equal to 2 (Singh et al., 2021a).

Table 3. Optical band gap energies, and Urbach energies of $Ge_{30}Se_{(70-x)}As_x$ (2,4,6, and 8) glasses

x	Optical bandgap energy (E_g) (eV)	Urbach energy (ΔE) (eV)
2	2.17	0.40
4	2.08	0.46
6	1.98	0.48
8	1.86	0.64

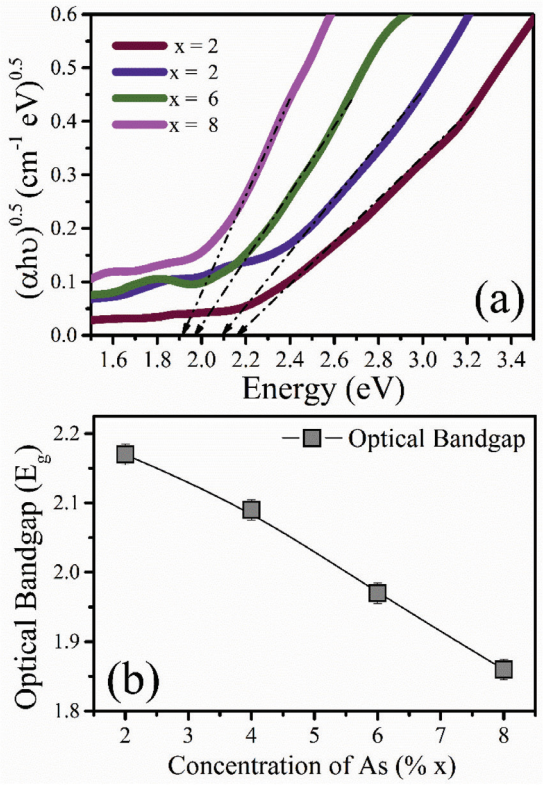

Figure 6. (a) Tauc's plot of studied samples, (b) variation of E_g with arsenic content(x)

By graphing the fluctuation of $(\alpha h\upsilon)^{1/2}$ vs hυ and extrapolating the linear region to the x-axis where α = 0 of the curves, optical energy band gap values can be determined using a Tauc's approach. The E_g values found for glasses with different concentrations of arsenic are displayed in Figure 6(b) and also summarized in Table 3. An increase in arsenic content is assumed to cause the band gap energy to fall by 2.17 to 1.86 eV, as found in earlier studies (Lal et al., 2019, El Ghandoor et al., 2012). The increase in Urbach energy levels may be the cause of this declining E_g value.

Investigating the disorder in the material is carried out using an essential technique known as the Urbach energy (ΔE). It is hypothesized that conduction and valence bands, as well as the width of the band tail (ΔE), are generated by electron transitions between localized states, the densities of which are expected to vary on energy exponentially.

The energy emitted into the bandgap as a result of random potential changes in the material often follows an exponential pattern. The experimental tail comes from the same physical source regardless of the material's structure. Included in these items are localized states that reach into the restricted band-gap area. The Urbach energy (ΔE) is often measured to describe the degree of disorder in vitreous systems. Plotting ln(α) versus photon energy (Figure 7(a)) and applying the empirical relation yields the Urbach energy (ΔE) (Urbach, 1953):

$$\alpha(\upsilon) = \alpha_0 exp\left(\frac{h\upsilon}{\Delta E}\right) \qquad (9)$$

In Figure7(b), the obtained values of ΔE are displayed. Interestingly, it is noteworthy that Urbach energy increases with increasing amounts of arsenic integrated into the host matrix. The outcome implies that the addition of arsenic causes a progressive increase in faulty states or diseases, which lowers the E_g of the materials being studied. Previous studies have indicated an inverse relationship between the E_g and ΔE (Hota et al., 2023).

4. CONCLUSIONS

Several glass compositions with the composition $Ge_{30}Se_{(70-x)}As_x$ have been created as bulk samples in the current investigation. The lack of any distinct peaks or lines in the XRD patterns verifies the as-prepared glasses' amorphous condition. The glass density increases when the arsenic content rises, whereas the molar volume (V_m) drops. By utilizing the measured values of ultrasonic

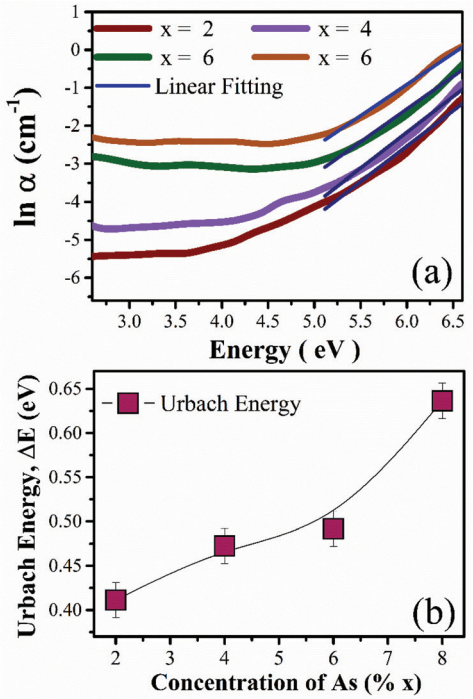

Figure 7. (a) variation of ln (α) against hν (b) variation of ΔE with arsenic content(x)

velocities (v_L, v_T) and density (ρ), the shear (S) and longitudinal (L) strains have increased from 11.30-11.40 Gpa and 32.54-32.71 Gpa, respectively. Next, the glasses' Poisson's ratio (Pr) and elastic moduli (K, H, and Y) were ascertained. It is discovered that the elastic modulus increases as the concentration of arsenic rises. An improvement in the materials' elastic characteristics has been demonstrated by the increase in elastic moduli values. All the thermal parameters are found to maintain a decreasing trend with the increasing arsenic content. The thermal stability (ΔT) of the glasses has been determined and is found to increase from 137-152K, indicating the thermally stable glassy system. The increasing trend of measured Urbach energy values results in the reduction of band gap energies from 2.17 to 1.86 eV, which indicates the applicability of these as-prepared samples absorbing layers in photovoltaic devices.

5. REFERENCES

1. BHUTTO, Y. A., PANDEY, A. K., SAIDUR, R., SHARMA, K. & TYAGI, V. V. 2023. Critical insights and recent updates on passive battery thermal management system integrated with nano-enhanced phase change materials. *Materials Today Sustainability,* 23**,** 100443.
2. BISWAS, D., DAS, A. S., MONDAL, R., BANERJEE, A., DEB, D., DUTTA, A., BHATTACHARYA, S., KABI, S. & SINGH, L. S. 2020. Study of microstructure and electrical conduction mechanisms of quaternary semiconducting glassy systems: Effect of mixed modifiers. *Journal of Non-Crystalline Solids,* 542**,** 120104.
3. BISWAS, D., MONDAL, R., MANDAL, D. & MONDAL, S. 2023. Investigation on Bi-induced changes on linear and non-linear optical parameters of As45-Se (55-x)-Bix chalcogenide glasses for photonic application. *Journal of Non-Crystalline Solids,* 614**,** 122401.
4. BOUKHRIS, I., KEBAILI, I., ZNAIDIA, S., NEFFATI, R., HEGAZY, H. H., ALY, K. A., MEHTA, N. & DAHSHAN, A. 2020. Optical constants of Sn-doped amorphous Ge-As-Te thin films and their physical characterization. *Physica B: Condensed Matter,* 583**,** 412066.
5. CHAHAL, S. & RAMESH, K. 2022. Glass formation, thermal stability and fragility minimum in Ge-Te-Se glasses. *Materials Research Bulletin,* 152**,** 111833.
6. CHAUHAN, J., KALRA, Y. & SINHA, R. K. 2023. Chalcogenide glass-based Low Loss Graded Index Photonic Crystal Fiber for non-linear applications in the Mid-IR regime. *Results in Optics,* 12**,** 100431.
7. CHOYON, A. K. M. S. J. & CHOWDHURY, R. 2022. Multifunctional chalcogenide (As2S3, As2Se3) dual-core photonic crystal fiber with elliptical air-hole for mid-IR optical communications: Design and analysis. *Optik,* 258**,** 168857.
8. DAVIS, E. A. & MOTT, N. F. 1970. Conduction in non-crystalline systems V. Conductivity, optical absorption and photoconductivity in amorphous semiconductors. *The Philosophical Magazine: A Journal of Theoretical Experimental and Applied Physics,* 22**,** 0903-0922.
9. DELAIZIR, G., DUSSAUZE, M., NAZABAL, V., LECANTE, P., DOLLÉ, M., ROZIER, P., KAMITSOS, E. I., JOVARI, P. & BUREAU, B. 2011. Structural characterizations of As–Se–Te glasses. *Journal of Alloys and Compounds,* 509**,** 831-836.
10. EL-DENGLAWEY, A., DAHSHAN, A., ALY, K. A. & SADDEEK, Y. B. 2021. Elastic moduli and theoretical estimations of physical properties of Ge3Se7–As2Te3. *Current Applied Physics,* 31**,** 214-220.
11. EL GHANDOOR, H., ZIDAN, H. M., KHALIL, M. M. H. & ISMAIL, M. I. M. 2012. Synthesis and Some Physical Properties of Magnetite (Fe3O4) Nanoparticles. *International Journal of Electrochemical Science,* 7**,** 5734-5745.
12. HAFIZ, M. M., OTHMAN, A. A., ELNAHASS, M. M. & AL-MOTASEM, A. T. 2007. Composition and electric field effects on the transport properties of Bi doped chalcogenide glasses thin films. *Physica B: Condensed Matter,* 390**,** 286-292.

13. HASSANIEN, A. S., NEFFATI, R. & ALY, K. A. 2020a. Impact of Cd-addition upon optical properties and dispersion parameters of thermally evaporated CdxZn1-xSe films: Discussions on bandgap engineering, conduction and valence band positions. *Optik,* 212**,** 164681.
14. HASSANIEN, A. S. & SHARMA, I. 2024. Synthesis, analysis, and characterization of structural and optical properties of thermally evaporated chalcogenide a-Cu-Zn-Ge-Se thin films. *Materials Chemistry and Physics,* 311**,** 128524.
15. HASSANIEN, A. S., SHARMA, I. & AKL, A. A. 2020b. Physical and optical properties of a-Ge-Sb-Se-Te bulk and film samples: Refractive index and its association with electronic polarizability of thermally evaporated a-Ge15-xSbxSe50Te35 thin-films. *Journal of Non-Crystalline Solids,* 531**,** 119853.
16. HOTA, S. B., ROY, D., GHOSH, B. K., DAS, A. S., MONDAL, R., KABI, S., CHAKRABARTI, C. & BISWAS, D. 2023. Effect of transition metal and alkali oxides on structural, optical and dielectric properties in Zinc-Phosphate amorphous glassy systems. *Journal of Non-Crystalline Solids,* 609**,** 122235.
17. KANG, S., FU, Y., GU, H. & LIN, C. 2022. Chalcogenide glass for thermoelectric application. *Journal of Non-Crystalline Solids: X,* 15**,** 100111.
18. KHAFAGY, A. H., ABO-GHAZALA, M., EL-ZAIDIA, M. M. & AMMAR, A. A. 1991. Internal friction in Se-Sb glasses. *Journal of Materials Science,* 26**,** 3477-3480.
19. KIBLER, B., SERRANO, E., MALDONADO, A., ROBICHAUD, L. R., DUVAL, S., BERNIER, M., BIZOT, R., DÉSÉVÉDAVY, F., VALLÉE, R., MESSADDEQ, Y. & SMEKTALA, F. 2023. All-fiber 2–6 μm coherent supercontinuum source based on chalcogenide fibers pumped by an amplified mid-IR soliton laser. *Optics Communications,* 542**,** 129568.
20. KUMAR, A., SHUKLA, R. K., KUMAR, A. & GUPTA, R. 2019. Light induced effects & defects in chalcogenide glassy semicoductors: A review. *Infrared Physics & Technology,* 102**,** 103056.
21. LAL, A., LOHIA, P. & DWIVEDI, D. K. 2019. Investigations of physical parameters of Ge doped binary Se-As chalcogenide glassy alloys for optical fiber application. *Materials Today: Proceedings,* 17**,** 338-344.
22. LEE, J. H., KIM, H., YOON, I. J., LEE, J. I., KO, S. Y. & CHOI, Y. G. 2021. Influence of oxygen incorporation on infrared transmission of ternary Ge-Sb-Se chalcogenide glass in the compositional range for use in infrared-imaging applications. *Ceramics International,* 47**,** 34633-34638.
23. MOHAMED, S. K., ABD EL-RAHEEM, M. M., WAKKAD, M. M., ABDEL HAKEEAM, A. M. & MOHAMED, H. F. 2023. Structural, optical, and electrical characteristics of Ge18Bi4Se78 chalcogenide glass for optoelectronic applications. *Memories - Materials, Devices, Circuits and Systems,* 6**,** 100085.
24. MONDAL, R., BISWAS, D., PAUL, S., DAS, A. S., CHAKRABARTI, C., ROY, D., BHATTACHARYA, S. & KABI, S. 2021a. Investigation of microstructural, optical, physical properties and dielectric relaxation process of sulphur incorporated selenium–tellurium ternary glassy systems. *Materials Chemistry and Physics,* 257**,** 123793.
25. MONDAL, R., MONDAL, S., TUDU, P., CHATTERJEE, P., KABI, S., DAS, A. S., CHATTOPADHYAY, S. & BISWAS, D. 2023. Tunable band gap, CB and VB positions of multicomponent Se65-xTe20Ge15Snx chalcogenide glassy systems: Effect of metallic additives on physical and optical parameters. *Materials Chemistry and Physics,* 296**,** 127187.
26. MONDAL, R., SINGH, Y. B., DAS, A. S., KABI, S., SINGH, L. S. & BISWAS, D. 2021b. Effect of Zn incorporation on physical properties of quaternary 0.7Se–0.2Ge–(0.1-x)Sb–xZn chalcogenide system: A theoretical prediction. *Physica B: Condensed Matter,* 612**,** 412896.
27. NIAN, S., ZHANG, Y., LI, J., ZHOU, N. & ZOU, W. 2018. Glass formation and properties of sodium zinc phosphate glasses doped with ferric oxide. *Advances in Applied Ceramics,* 117**,** 319-327.
28. OTA, R., YAMATE, T., SOGA, N. & KUNUGI, M. 1978. Elastic properties of Ge-Se glass under pressure. *Journal of Non-Crystalline Solids,* 29**,** 67-76.
29. PAL, S. K., CHANDEL, N. & MEHTA, N. 2019. Synthesis and thermal characterization of novel phase change materials (PCMs) of the Se–Te–Sn–Ge (STSG) multi-component system: calorimetric studies of the glass/crystal phase transition. *Dalton Transactions,* 48**,** 4719-4729.
30. PITCHAPPA, P., KUMAR, A., PRAKASH, S., JANI, H., VENKATESAN, T. & SINGH, R. 2019. Chalcogenide Phase Change Material for Active Terahertz Photonics. *Advanced Materials,* 31**,** 1808157.
31. SADDEEK, Y. B., ISSA, S. A. M., ALHARBI, T., ALY, K., AHMAD, M. & TEKIN, H. O. 2020. Mechanical and nuclear shielding properties of sodium cadmium borate glasses: Impact of cadmium oxide additive. *Ceramics International,* 46**,** 2661-2669.
32. SADDEEK, Y. B., YAHIA, I. S., ALY, K. A. & DOBROWOLSKI, W. 2010. Spectroscopic, mechanical and magnetic characterization of some bismuth borate glasses containing gadolinium ions. *Solid State Sciences,* 12**,** 1426-1434.

33. SHUKLA, M. K. & SHARMA, K. 2019. Improvement in mechanical and thermal properties of epoxy hybrid composites by functionalized graphene and carbon-nanotubes. *Materials Research Express,* 6**,** 125323.
34. SINGH, Y. B., BISWAS, D., SHAH, S. K., SHAW, S., MONDAL, R., DAS, A. S., KABI, S. & SINGH, L. S. 2021a. Investigation of optical properties and electrical conductivity mechanism of Fe2O3–Sm2O3–ZnO–P2O5 quaternary glass nanocomposite systems. *Materialia,* 15**,** 100963.
35. SINGH, Y. B., CHATTERJEE, P., NINGTHEMCHA, R. K. N., ADHIKARI, S., MONDAL, R., DAS, A. S., KABI, S., SINGH, L. S. & BISWAS, D. 2021b. Compositional dependence of structural, physical, and, in particular, optical parameters of Se50–xTe30Sn20Sbx chalcogenide glassy systems. *Materials Chemistry and Physics,* 274**,** 125153.
36. URBACH, F. 1953. The Long-Wavelength Edge of Photographic Sensitivity and of the Electronic Absorption of Solids. *Physical Review,* 92**,** 1324-1324.
37. VASHIST, P., PATIAL, B. S. & THAKUR, N. 2022. Synthesis and investigation of topological behaviour and structural modification in Se-Te-Ge-Bi nanostructured alloys. *Applied Surface Science Advances,* 8**,** 100220.
38. WANG, X., WANG, C. & DAI, S. 2023. Chalcogenide glass-tapered fiber sensor modified by graphene oxide doped with platinum nanoparticles for high-sensitivity measurement. *Results in Physics,* 47**,** 106348.
39. YADAV, A., KUMAR, A., SHARMA, K. & SHUKLA, M. K. 2019. Investigating the Effects of Amine Functionalized Graphene on the Mechanical Properties of Epoxy Nanocomposites. *Materials Today: Proceedings,* 11**,** 837-842.
40. YANG, G., BUREAU, B., ROUXEL, T., GUEGUEN, Y., GULBITEN, O., ROILAND, C., SOIGNARD, E., YARGER, J. L., TROLES, J., SANGLEBOEUF, J.-C. & LUCAS, P. 2010. Correlation between structure and physical properties of chalcogenide glasses in the. *Physical Review B,* 82**,** 195206.